Supporting Information

Molecular-level understanding of protein adsorption at the interface between water and a strongly-interacting uncharged solid surface

Matthew J. Penna, Milan Mijajlovic and Mark J. Biggs*

School of Chemical Engineering, The University of Adelaide, Adelaide, Australia, 5005.

1. METHOD IN DETAIL

The Pt(111) and Au(111) surfaces were created following Heinz *et al.*[1,2] using the lattice constants of a = 3.9236 Å and 4.0782 Å respectively. The surfaces were assumed rigid throughout the work reported here. In the vast majority of the work reported here, the interaction between the metal surface and the solution phase above was modeled using a Lennard-Jones potential with the potential parameters of Heinz *et al.*,[1,2] which are summarized in Table 1 below. The polarizable gold potential of Iori, Corni and co-workers[3,4] was also used to establish if a major change in the form of the surface model affected the adsorption mechanism identified using the LJ model.

Table S1. Lennard-Jones parameters used for the metal surfaces considered here

Parameter	Gold	Platinum
σ (Å)	2.951	2.845
ε (kcal/mol)	5.29	7.8

The surface was solvated with TIP3P water molecules[5] before the height of the simulation cell was adjusted marginally to ensure that the density of the water more than 15 Å from the surface was equal to that of a water-only NPT simulation at 298K and 1 atm. The simulation cells, which had periodic boundary conditions applied to them in all three dimensions, were 48.05 × 52.706 × 82.5 Å^3 and 59.937 × 57.674 × 75 Å^3 in size for SD152 and A3 respectively.

For each peptide, the zwitterionic form was created using the *Molefacture* function in VMD[6] and solvated in a periodic cell with around 1900 and 6000 TIP3 water molecules[5] for SD152 and A3 respectively. Using NAMD,[7] theses system were minimized for 1000 time-steps at 0 K, heated to 298 K then subject to a 1ns MD simulation in the NPT ensemble at 298 K and 1 atm. The initial peptide conformations for the adsorption simulations were randomly selected from the later part of the NPT simulations.

For each adsorption simulation, the peptide conformation taken from the NPT bulk phase MD simulation was inserted centrally in the water volume above the solid surface with a randomly selected orientation such that no part of it was within 12 Å of the surface. Water molecules within 2 Å of the peptide were removed leaving approximately 5700 and 7000 water molecules in the SD152 and A3 systems respectively. Sodium and chlorine ions were added to give a NaCl concentration of 0.15 mol. Using NAMD,[7] the systems were minimized for 1000 steps at 0 K before being heated to 298 K. During heating, the center of mass of the peptide was constrained to ensure no peptide atom was within 12 Å of the surface.

All adsorption simulations were performed using NVT MD as implemented in NAMD.[7] The temperature was fixed at 298 K using a Langevin thermostat[8] with a damping coefficient of 5 ps^{-1}. The Shake algorithm[9] was employed to fix the lengths of all bonds involving hydrogen atoms to allow a 2 fs timestep to be used. The CHARMM49 forcefield[10] was used in conjunction with the TIP3P water model.[5] Long range electrostatic interactions were calculated using by the particle-mesh Ewald method with a grid spacing of 1.0 Å. A cut-off radius of 12 Å was used for the short range (*i.e.* Lennard-Jones) interaction with a switching implemented at 10 Å. Coordinates of all the atoms in the system were written out every 1 ps (500 time-steps) for subsequent analysis.

2. ADDITIONAL RELEVANT RESULTS AND ANALYSIS

2.1 Movie of trajectory of Figure 2

A movie showing the trajectory in Figure 2 is provided with this report. It has been annotated so as to allow the reader to identify the key events in the trajectory identified in Figure 1.

2.2 Quantitative analysis of biased diffusion

We demonstrate here quantitatively the biased diffusion by comparing the 'ensemble' average velocity of the Sd152 peptide towards the surface during this phase, v_{bz}, with the 'ensemble' average velocity components parallel to the surface, v_{bx} and v_{by}. The ensemble averages were generated using average peptide velocity data derived from 20 of the SD152 simulations where the biased diffusion was observed to start with no part of the peptide within 20 Å of the solid surface, a distance selected on the basis that this would exclude any influence of the dispersion interactions arising from the layered water, which at most projects around 8 Å into the solution (see Figure 2 of the main paper); the total number of SD152 simulations used in the ensemble average was selected to give stable averages with modest uncertainties. The average velocity components for each simulation were obtained by fitting a straight line through the displacement *vs.* time data for the entire period of the biased diffusion phase as illustrated in Figure S1.

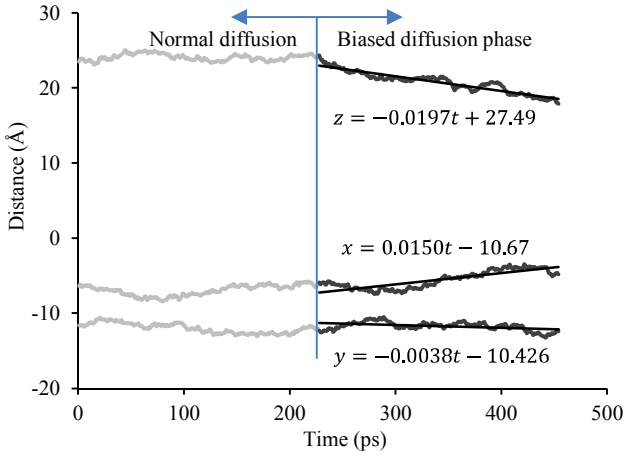

Figure S1. Example of the method for determining the average of the velocity components of the peptide in the biased diffusion phase. These average velocity component values were then averaged across 20 simulations to obtain an 'ensemble' average and standard deviation, which are shown in Table S2.

As can be seen from Table S2, which shows the ensemble average velocity components from the analysis outlined above, the velocity components parallel to the surface during the biased diffusion phase are statistically zero. The velocity normal towards the surface, however, is clearly statistically non-zero.

Table S2. Ensemble average and standard deviation of SD152 peptide velocity components for the biased diffusion phase (see text above for explanation of averaging process)

Component	Average	Standard deviation
v_{bx} (m/s)	0.087	1.081
v_{by} (m/s)	0.001	0.832
v_{bz} (m/s)	3.225	0.958

2.3 Water density around peptide

Figure S2 shows that, like the solid surface, the peptide is also surrounded by at least one if not two layers of somewhat peptide-bound water as evidenced. These water layers make the peptide in effect larger than one would otherwise think.

The profile in Figure S2 was obtained from a simulation of the SD152 peptide in a water box sufficiently large such that the water shell surrounding the peptide did not interact with the water shells of the periodic images. Simulations were performed in the NPT ensemble at 298 K and 1 atm. The dynamics of the peptide was not restricted during the simulation. The profile was built by sampling over time the water distribution around the peptide. This involved generating a profile for each snapshot saved in the simulation and then taking their average (*i.e.* summing them and dividing through by the total number of snapshots). The profile for a snapshot was obtained by superimposing on the peptide a 3D grid of 0.2 Å spacing and then determining the normal distance of each cell in the grid from the molecular surface of the peptide along with the number of water molecules in the cells relative to the total in the simulation volume.

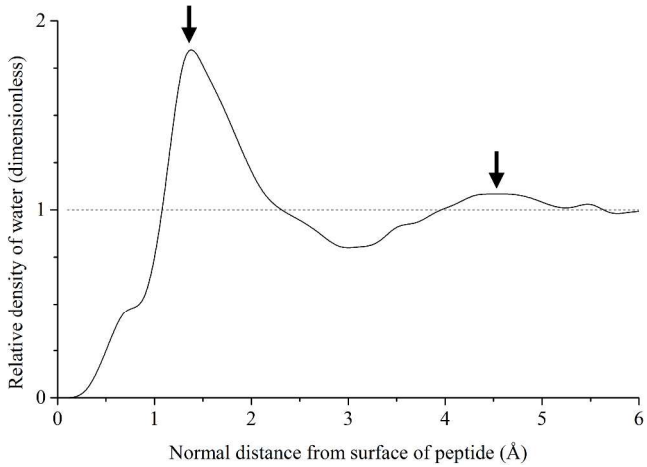

Figure S2. Variation of the water density (relative to the bulk density) with normal distance from the surface of the SD152 peptide; the centers of the two water layers bound to the peptide are indicated with arrows.

2.4 Distribution of time for initiation of lockdown for the A3 peptide

The counterpart of Figure 5 for peptide A3 is shown here in Figure S3.

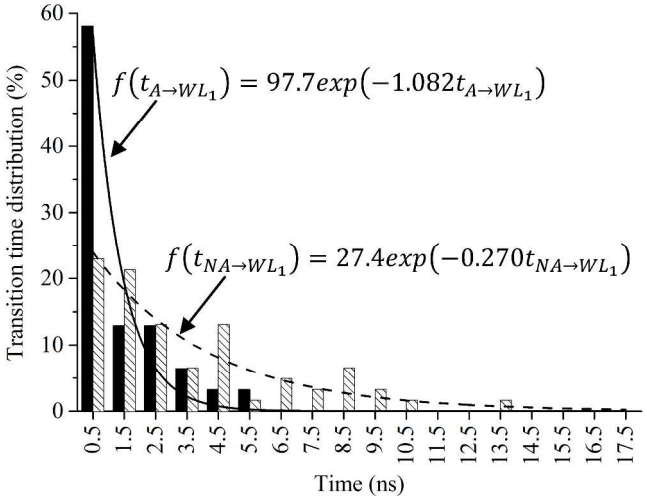

Figure S3. Distribution of the time for A3's anchor groups (black bars = statistics from the simulations; line = exponential fit) and non-anchor groups (hashed bars = statistics from the simulations; broken line = exponential fit) to transition from the second water layer into the water layer immediately adjacent to the solid surface when initiating lock-down, $t_{A\rightarrow WL_1}$ and $t_{NA\rightarrow WL_1}$ respectively. There are 92 lockdown initiation events net.

2.5 Probability of a residue following the lockdown initiator as a function of distance from it for the A3 peptide

The counterpart of Figure 7 for peptide A3 is shown here in Figure S4.

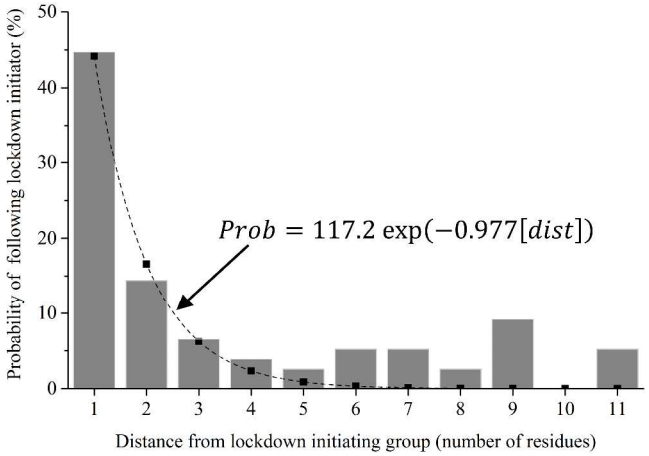

Figure S4. Probability of a group following the lockdown initiator into the adsorbed state as a function of its 'distance' from the initiator (in residues) for the A3 peptide. The total number of events are 76. The statistics derived from the ensemble of simulations are shown as bars and the fit as a broken line with points.

2.6 Probability of the third residue following the second lockdown residue

As seen in Figure S5, the probability of the third residue following the second residue into lockdown is exponentially related to its distance from the second residue. Comparison of these two plots with Figure 7 and Figure S4 respectively shows this is qualitatively the same as for the second residue to follow the residue that initiates lockdown.

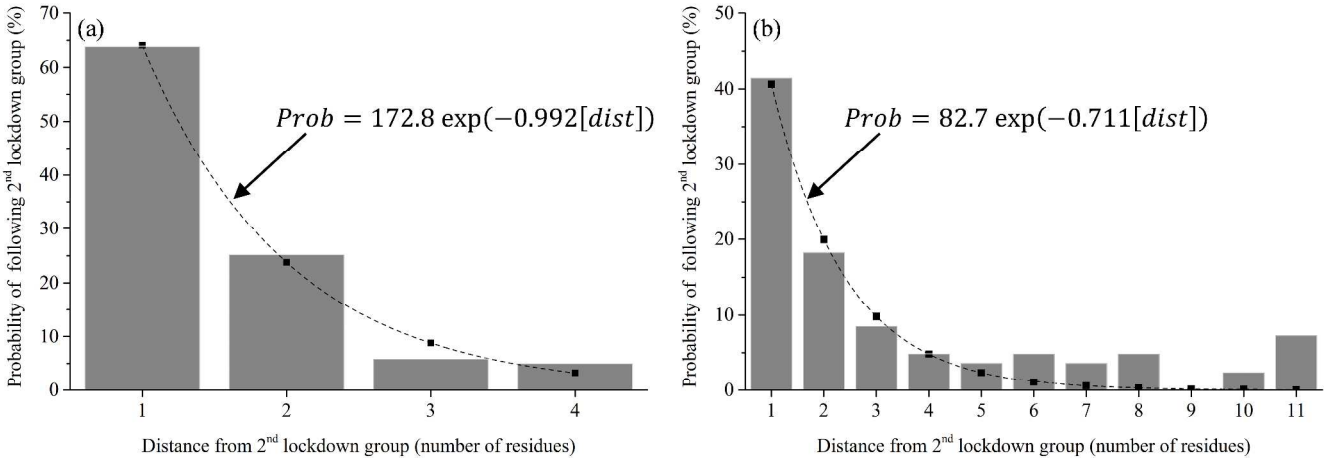

Figure S5. Probability of the third group following the second lockdown group into the adsorbed state as a function of its 'distance' from this second group (in residues): (a) SD152; (b) A3. The total number of events are 119 and 82 respectively. The statistics derived from the ensemble of simulations are shown as bars and the fit as a broken line with points.

2.7 Mean square displacements and self-diffusion coefficients

Figure S6 below shows the mean square displacement (MSD) of the peptide center of mass (CoM) for the two peptides in the bulk, when anchored, at and soon after initiation of lockdown (defined as when the number of peptide atoms in contact with the surface is between 1 and 10 inclusive), and throughout lockdown (defined as when the number of peptide atoms in contact with the surface is more than 10).

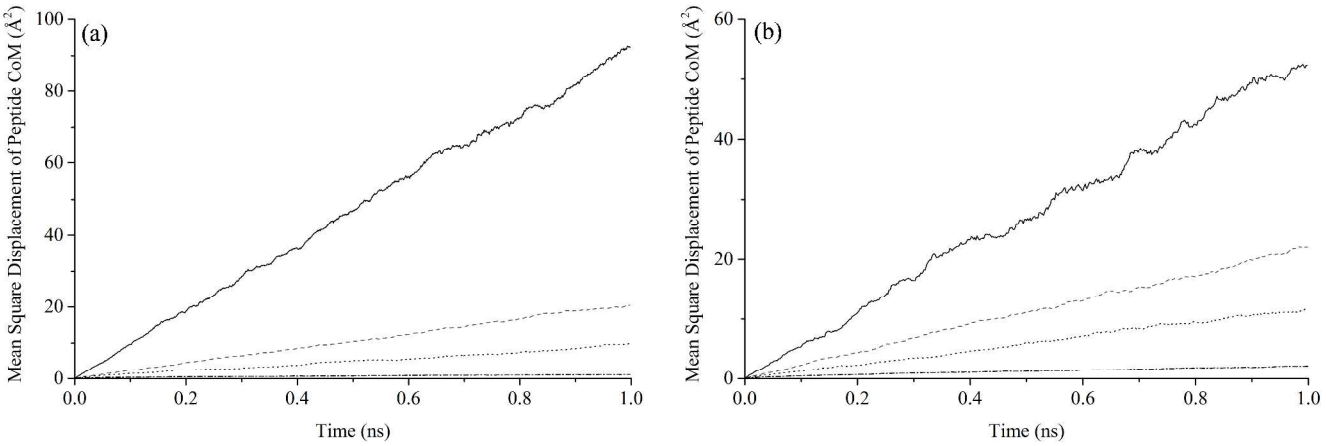

Figure S6. Mean square displacement for the peptides in the bulk phase (thick solid line), during the anchor phase (broken line), following initiation of lockdown (dotted line), and throughout lockdown (broken-dotted line): (a) SD152, and (b) A3.

The diffusion coefficient for each phase in Figure S6 has been estimated using the Einstein relation

$$D = \lim_{t\to\infty} \frac{1}{2d} \frac{MSD}{t}$$

where d is the dimension (d = 3 for the bulk phase, and d = 2 for the surface phases), and t the time. The values are shown in Table 1 of the main paper.

2.8 Comparison of Lennard-Jones gold and polarizable gold surfaces

Whilst, as discussed in the main paper, the exact potential models adopted for the peptide and water are unlikely to change the fundamentals of the findings derived here, the same could not be ruled out *a priori* for the surface, particularly the possible influence of electron polarization which is, of course, not explicitly captured in the Lennard-Jones (LJ) surface models that underpin the main findings here. We, therefore, replicated in a reduced form (around one-third the number of simulations) the study of A3 on gold using the polarizable gold surface model of Corni and co-workers.[12,13] Whilst the more limited nature of this adjunct study means we cannot draw definitive conclusions about individual groups, comparison at the group-type level (i.e. polar/non-polar) is possible – we do this below.

Firstly, as with the study based on the LJ surface, biased diffusion towards the surface was observed in all simulations involving the polarizable gold surface. Analysis of the oxygen and hydrogen density distributions in the water normal to the surface reveals spatial and orientational ordering also exists for the polarizable surface, although it is not as strong or tightly bound. As with the LJ surface, this structuring endows the interface with charged layers that are the origin of the biased diffusion identified using the LJ surface.

Figure S7 shows the anchoring propensities for the side-chain groups and termini for A3 on the polarizable gold surface. Whilst comparison of this figure with its counterpart, Figure 4(b) in the main paper, reveals some differences between the anchoring propensities at the individual side-chain level, fundamentally the trends are the same for the two surface models. For both surfaces 4 of the 5 hydrophilic groups are located in the top 8 anchors with the strongly interacting sulfur-containing Met and ring-containing Phe side-chains also sitting in this group for both surfaces. Meanwhile, the bottom 8 anchors for both surfaces are dominated by hydrophobic side-chains (7 and 6 for the LJ and polarizable surfaces respectively).

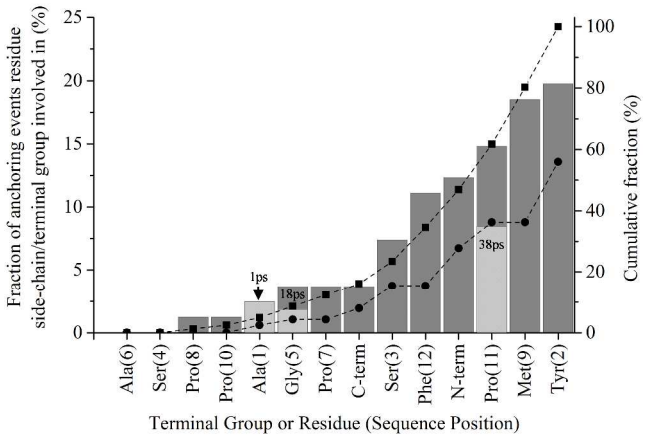

Figure S7. Fraction of anchoring events for terminal/residue side-chain groups of A3 on the polarizable gold surface of Corni and co-workers.[12,13] The total number of anchoring events is 81. The groups are shown left to right in increasing *net* fraction. The hydrophobic group bars are split: where the group is accompanied (11) by a hydrophilic group (light grey with average time to accompaniment shown in ps) or not. The cumulative fraction for net (■) and hydrophilic group-associated events (●) are also shown.

Figure S8 shows the lockdown initiating propensities for the side-chain groups and termini for A3 on the polarizable gold surface. Comparison of this figure with Figure 6(b) shows that, once again, fundamentally the trends are the same, with the top-8 being dominated by hydrophilic groups (relative to their total number) and the stronger interacting hydrophobic groups (Met and Phe), whilst the bottom-8 are in turn dominated by the weaker interacting hydrophobic groups.

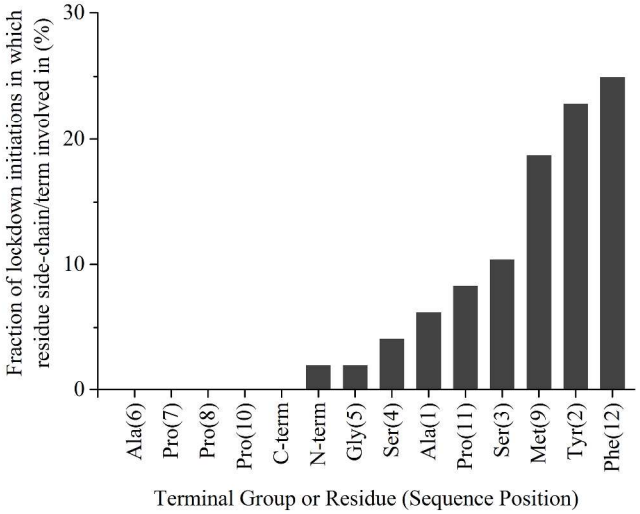

Figure S8. Fraction of stable lockdown initiation events for the terminal/residue side-chain groups of A3 on the polarizable gold surface of Corni and co-workers.[12,13] There were 48 stable lockdown initiation events; as only 5 dynamic events were observed in this limited study, these have been omitted.

The limited study using the polarizable gold surface model prevents us claiming with certainty that the individual groups for this surface behave exactly the same as for the LJ surface. However, the above analysis indicates that the essentials of the mechanism as outlined in Figure 1 of the main paper and the associated details of each phase, including the origins of the biased diffusion and what makes a good anchor and lockdown initiator – namely groups containing hydrophilic parts, sulfur or rings (excluding Pro) – are supported despite use of the fundamentally different polarizable surface.

REFERENCES

1. Heinz, H.; Vaia, R. A.; Farmer, B. L.; Naik, R. R. *J. Phys. Chem. C* **2008**, *112*, 17281.
2. Heinz, H.; Farmer, B. L.; Pandey, R. B.; Slocik, J. M.; Patnaik, S. S.; Pachter, R.; Naik, R. R. *J. Am. Chem. Soc.* **2009**, *131*, 9704.
3. Iori, F.; Corni, S. *J. Comput. Chem.* **2008**, *29*, 1656.
4. Iori, F.; Di Felice, R.; Molinari.; Corni, S. *J. Comput. Chem.* **2009**, *30*, 1465.
5. Jorgensen, W. L.; Chandrasekhar, J.; Madura, J. D.; Impey, R. W.; Klein, M. L. *J. Chem. Phys.* **1983**, *79*, 926.
6. Humphrey, W.; Dalke, A.; Schulten, K. (1996). *J. Molec. Graphics*, *14*, 33.

7. Phillips, J. C.; Braun, R.; Wang, W.; Gumbart, J.; Tajkhorshid, E.; Villa, E.; Chipot, C.; Skeel, R. D.; Kale, L.; Schulten, K. *J. Comput. Chem.* **2005**, *26*, 1781.
8. McQuarrie, D. A. *Statistical Mechanics*, Harper Collins Publishers, New York, 1976.
9. Ryckaert, J. P.; Ciccotti, G.; Berendsen, H. J. C. *J. Comput. Phys.* **1977**, *23*, 327.
10. MacKerell, A. D.; Bashford, D.; Bellott, R. L.; Dunbrack, R. L.; Evanseck, J. D.; Field, M. J.; Fischer, S.; Gao, J.; Guo, H.; Ha, S.; Joseph-McCarthy, D.; Kuchnir, L.; Kuczera, K.; Lau, F. T. K.; Mattos, C.; Michnick, S.; Ngo, T.; Nguyen, D. T.; Prodhom, B.; Reiher, W. E.; Roux, B.; Schlenkrich, M.; Smith, J. C.; Stote, R.; Straub, J.; Watanabe, M.; Wiorkiewicz-Kuczera, J.; Yin, D.; Karplus, M. J. *J. Phys. Chem. B* **1998**, *102*, 3586.
11. A hydrophilic group is deemed to have 'accompanied' a non-polar anchor if it enters the second water layer within no more than 100 ps of the anchoring occurring. This period is based on a conservative estimate of the time that elapses between a hydrophilic group forming a 'strong' interaction (*e.g.* hydrogen bond) with the second water layer and it directly entering the water layer (*i.e.* it reflects the assertion that when a hydrophilic group accompanies a non-polar anchor, it is likely that the hydrophilic group is playing a major role in the anchoring).
12. Iori, F.; Corni, S. *J. Comput. Chem.* **2008**, *29*, 1656.
13. Iori, F.; Di Felice, R.; Molinari, E.; Corni, S. *J. Comput. Chem.* **2009**, *30*, 1465.